Surface shape resonances and surface plasmon polariton excitations in bottle-shaped metallic gratings

Diana C. Skigin* and Ricardo A. Depine†
Grupo de Electromagnetismo Aplicado, Departamento de Física, Facultad de Ciencias Exactas y Naturales, Universidad de Buenos Aires, Ciudad Universitaria, Pabellón I, 1428 Buenos Aires, Argentina
(Received 23 October 2000; published 27 March 2001)

We study surface plasmon polariton excitations and surface shape resonances in a lossy metallic grating with bivalued cavities. The modal formalism is used to solve the diffraction problem for the infinite grating and the homogeneous problem for a single cavity in a plane surface. Both polarization modes are considered. We provide curves of reflected efficiency versus wavelength as well as near-field plots. The resonances are identified as dips in the reflected efficiency, which imply significant power absorptions. Results for various depths of the cavities and for several angles of incidence are shown, where the different types of resonant behavior can be appreciated. Particular attention is paid to the changes introduced by the finite conductivity of the metal in relation to the results obtained for a perfect conductor.

DOI: 10.1103/PhysRevE.63.046608 PACS number(s): 42.25.−p

I. INTRODUCTION

It is well known that when an infinite metallic grating is illuminated by *p*-polarized light, a surface plasmon polariton (SPP) can be excited along the surface [1]. This excitation is accompanied by a significant power absorption [2,3], and consequently it produces a sudden change in the efficiency curves of the reflected orders. For a given period and material of the grating, and for a fixed angle of incidence, the excitation of a SPP is produced for a particular wavelength at which one of the diffracted orders propagates parallel to the surface, and therefore, the electric field near the surface is intensified. This phenomenon is particularly important when the corrugations are shallow. As the depth of the grooves is increased, another type of resonance can take place: the eigenmodes of each cavity can be excited, producing interesting resonant effects, such as field enhancement inside the corrugations [4–6]. Contrary to the SPP excitations, these resonances are associated with the particular shape of each groove and can be excited by *s*-polarized light [7–9], independently of the period of the grating and the angle of incidence. They are usually called surface shape resonances (SSRs). Both effects manifest themselves as dips in the reflected and absorbed power curves, and they can even merge into one another forming hybrid resonances [10].

To identify the SSRs it is important to perform an independent calculation of the waveguide modes of the cavities so that the dips are distinguished from other effects that arise in infinite gratings. The solution of the homogeneous problem—the scattering problem from a single cavity without incident field—gives us a good estimation of the resonant wavelengths [6,11].

The only experimental evidence of the SSR excitations was recently given by López-Rios *et al.* [10], for lamellar gratings. In Ref. [10] the authors compare experimental results for a gold grating with numerical computations based on the transfer matrix formalism, for *p*-polarized incident light. By varying the depth of the cavities, they analyze the evolution of the resonances and show that for shallow corrugations the resonances correspond to the SPP type, and consequently the field is weak in the groove and intense in the external surface. On the other hand, for deeper gratings the resonances are of SSR type where the electric field is mainly concentrated in the grooves and is practically zero in all other regions.

Taking into account that for *s*-polarized incident light we do not have SPP resonances but we do have SSR, gratings can be used in many applications based on selective processes, such as polarizers and filters. In particular, bivalued profiles of the grooves can yield more significant intensifications of the field and higher quality resonances than single-valued profiles [4,5], especially for *s* polarization. The resonant characteristics of volumes such as open cylinders had been studied by many authors [12–16] mainly for circular geometries. However, the ''bottle'' shape of the cavities considered in this paper provides us with advantages, such as, the freedom to vary the depths and widths independently, the ease to manufacture this kind of structures, and the simplicity of the modal formalism used to model the diffraction problem.

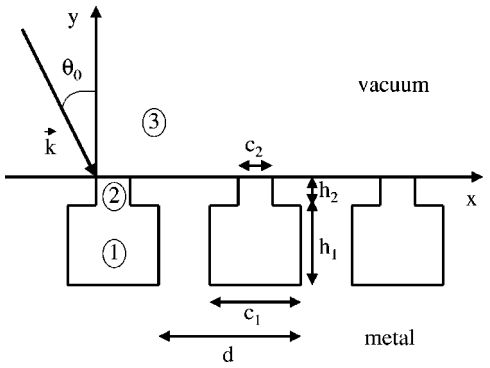

FIG. 1. The infinite grating made of bottle-shaped cavities in a metallic surface.

*Email address: dcs@df.uba.ar
†Email address: rdep@df.uba.ar

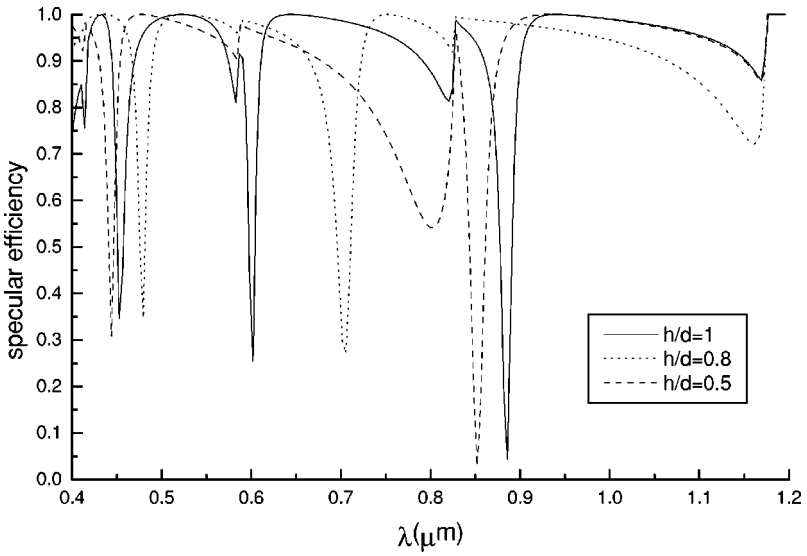

FIG. 2. Specular efficiency versus wavelength for a perfectly conducting grating of period $d=1$ μm with bottle-shaped grooves of width $c_1=0.35$ μm and $c_2=0.1$ μm, $h_1=0.9h$, $\theta_0=10°$ and p polarization, for three different values of the total depth h: 0.5, 0.8, and 1 μm.

The purpose of this paper is to provide numerical evidence of resonances in deep metallic gratings with multivalued corrugations. In a previous paper [6], we considered the ideal case of a perfectly conducting material and found interesting results that have led us to extend the study to the real case of a lossy metal. This extension, done by means of the surface impedance boundary condition (SIBC) [17], is presented in this paper. The variety of applications that come up from the numerical results also intend to encourage the design of experiments to measure these resonant properties.

In Sec. II we outline the modal method applied to the diffraction problem from an infinite metallic grating with bottle-shaped grooves, using the SIBC. We consider s and p polarizations of the incident plane wave. In Sec. III we pose the homogeneous problem for a single cavity in a metallic plane. The method is analogous to that presented in [6] for a perfectly conducting surface, so the reader is referred to the above reference for more details on the procedure. Some of the results of the numerical computations are shown and discussed in Sec. IV, where plots of reflected efficiency and near field are provided. Finally, concluding remarks are given in Sec. V.

II. DIFFRACTION FROM THE INFINITE GRATING

The grating consists of a periodic array of bottle-shaped one-dimensional cavities on a metallic surface, as shown in Fig. 1. The structure is illuminated by a plane wave of wavelength λ, whose wave vector $\vec{k}$ forms an angle θ_0 with the y axis, and the z axis coincides with the rulings direction. The complete problem is solved by separating the basic polarization cases: TE or s (electric field in the z direction) and TM or p (magnetic field in the z direction). Both scalar problems are solved using the modal approach, which provides us with a simple formulation for the present geometry. Each cavity has a wide part that we call ''body'' (region 1) and a narrow part referred to as ''neck'' (region 2). The body has width c_1 and height h_1, and the neck has width c_2 and height h_2 (see Fig. 1). The total depth of the rulings is $h=h_1+h_2$ and the period of the grating is d. The field in region 3($y\geqslant 0$) is the sum of the incoming plane wave and the diffracted field

$$f_3(x,y)=e^{i(\alpha_0 x-\beta_0 y)}+\sum_{n=-\infty}^{\infty}\mathcal{R}_n^q e^{i(\alpha_n x+\beta_n y)},\quad q=s,p \tag{1}$$

where (j denotes the region)

$$f_j(x,y)=\begin{cases}E_{zj}(x,y) & \text{in the } s \text{ mode}\\ H_{zj}(x,y) & \text{in the } p \text{ mode,}\end{cases} \tag{2}$$

$$\alpha_0=k\sin\theta_0, \tag{3}$$

$$\beta_0=k\cos\theta_0, \tag{4}$$

$$\alpha_n=\alpha_0+\frac{2\pi}{d}n, \tag{5}$$

$$\beta_n=\begin{cases}\sqrt{k^2-\alpha_n^2} & \text{if } k^2>\alpha_n^2\\ i\sqrt{\alpha_n^2-k^2} & \text{if } k^2<\alpha_n^2,\end{cases} \tag{6}$$

$k=|\vec{k}|=\omega/c=2\pi/\lambda$, i is the imaginary unit, and $\mathcal{R}_n^q$ are unknown complex amplitudes usually referred to as Rayleigh coefficients.

To account for the losses in the metallic substrate, we use the surface impedance boundary condition (SIBC) [17], which allows us to obtain the diffracted efficiencies and the fields inside the cavities without calculating the fields inside the metallic region. The expression of the SIBC is

$$\vec{E}_{\parallel}=\mathcal{Z}\hat{n}\times\vec{H}_{\parallel}, \tag{7}$$

where $\vec{E}_{\parallel}$ and $\vec{H}_{\parallel}$ are the tangential components of the electric and the magnetic field, respectively, $\hat{n}$ is the normal to the boundary surface and $\mathcal{Z}$ is the surface impedance. For highly conducting materials, $\mathcal{Z}$ can be approximated by $1/\nu$ (ν is the complex refraction index). This condition is applied to find the modal eigenfunctions in regions 1 and 2. In these zones the fields can be expressed as

TABLE I. Resonant wavelengths λ (μm) for a perfectly conducting rectangular waveguide, for p polarization.

n	$h=1$ μm	$h=0.8$ μm	$h=0.5$ μm
1	1.8	1.44	0.9
2	0.9	0.72	0.45
3	0.6	0.48	0.3
4	0.45	0.36	0.225

$$f_j(x,y)=\sum_{m=0}^{\infty} U_{m,j}^q(x)w_{m,j}^q(y), \quad q=s,p, \quad j=1,2 \quad (8)$$

where $U_{m,j}^q(x)$ and $w_{m,j}^q(y)$ are linear combinations of trigonometric functions of x and y, respectively, and depend on the polarization mode, as denoted by the superscript q (see the Appendix for the explicit expressions of these functions). These eigenfunctions involve unknown modal amplitudes A_m^q, a_m^q, and b_m^q, which are to be found by matching the fields at the interfaces $y=-h_2$ and $y=0$. The procedure followed here is essentially the same as that in Ref. [18] except for the fact that in the present case we have to match the fields at one more interface ($y=-h_2$). Thus, four systems of equations are generated for the four unknown vectors (three of modal amplitudes in regions 1 and 2 and the Rayleigh coefficients $\mathcal{R}_n^q$). After substitutions and matrix inversions we get a matrix equation for $\mathcal{R}_n^q$, and the reflected efficiencies (e_n^q) can be calculated as

$$e_n^q=|\mathcal{R}_n^q|^2\beta_n/\beta_0, \quad q=s,p. \quad (9)$$

III. EIGENMODES OF A METALLIC BOTTLE-SHAPED CAVITY

In this section we calculate the surface shape resonances of a bottle-shaped groove on a metallic plane. An indepen-

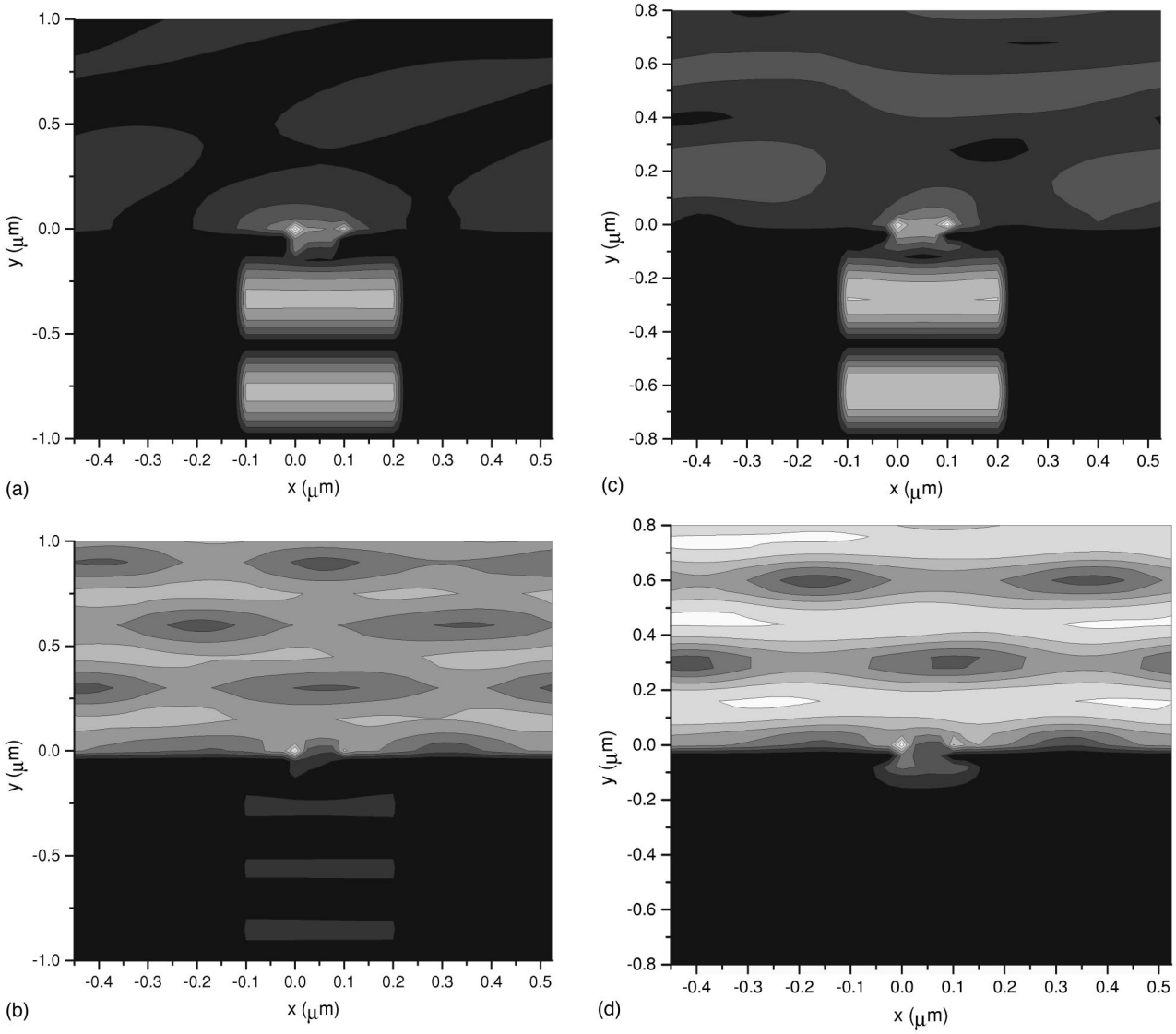

FIG. 3. Near electric field for the same grating of Fig. 2 and p polarization: (a) $h=1$ μm and $\lambda=0.885\,67$ μm, (b) $h=1$ μm and $\lambda=0.586\,67$ μm, (c) $h=0.8$ μm and $\lambda=0.7055$ μm, (d) $h=0.8$ μm and $\lambda=0.586\,67$ μm.

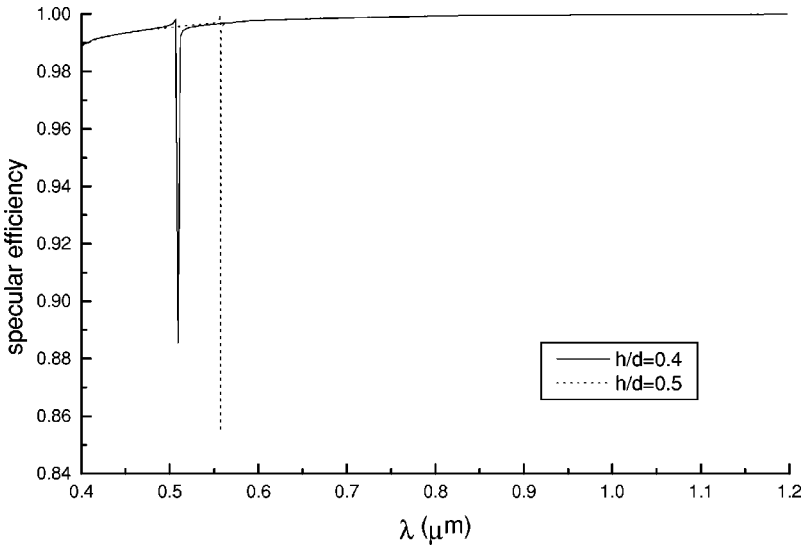

FIG. 4. Specular efficiency versus wavelength for a perfectly conducting grating of period $d=1$ μm with bottle-shaped grooves of width $c_1=0.35$ μm and $c_2=0.1$ μm, $h_1=0.9h$, $\theta_0=10°$ and *s* polarization, for two different values of the total depth h: 0.4 and 0.5 μm.

dent calculation of the resonant wavelengths of the cavities is essential to characterize the response of the grating, and to differentiate between surface shape resonances—associated with geometrical parameters of the cavity—and other types of anomalies. A good estimation of the SSR wavelengths can be obtained by the solution of the homogeneous problem, i.e., the scattering problem without incident field. Maradudin *et al.* [11] solved it for a rectangular cavity on a perfectly conducting plane.

The procedure followed in the present paper for lossy metals is the same as the one we used for a perfectly conducting structure of the same shape [6]. Even though interesting results were reported in [6], the perfect conductor is still an idealization and cannot account for effects such as selective absorption. Consequently, here we use the modal method in conjunction with the SIBC to solve the homogeneous problem of a single bottle-shaped one-dimensional cavity on a lossy metallic plane. The field in region 3 is thus expressed as

$$f_3(x,y)=\int_{-\infty}^{\infty}\mathcal{R}^q(\alpha)e^{i(\alpha x+\beta y)}d\alpha, \tag{10}$$

where $\mathcal{R}^q(\alpha)$ is an unknown function, and $\beta^2=k^2-\alpha^2$. In regions 1 and 2 the modal expansions have the same expressions as in the periodic grating case given in the Appendix, since the SIBC is also applied here. When matching the fields at $y=-h_2$ and at $y=0$, we obtain x-dependent equations. After projection in appropriate bases of functions and several substitutions, we obtain a homogeneous matrix equation for the unknown modal amplitudes of the body of the cavity, i.e., for A_m^q. This system has a nonzero solution if the determinant of the complex matrix vanishes. The sets of parameters $(\lambda,c_1,c_2,h_1,h_2,\nu)$ that make the determinant vanish correspond to resonant conditions, and consequently to surface shape resonances of the cavity. Since the matrix is complex, the roots of the determinant are also complex: the real part is related to the resonant parameter and the imaginary part is associated with the quality of the resonance. The

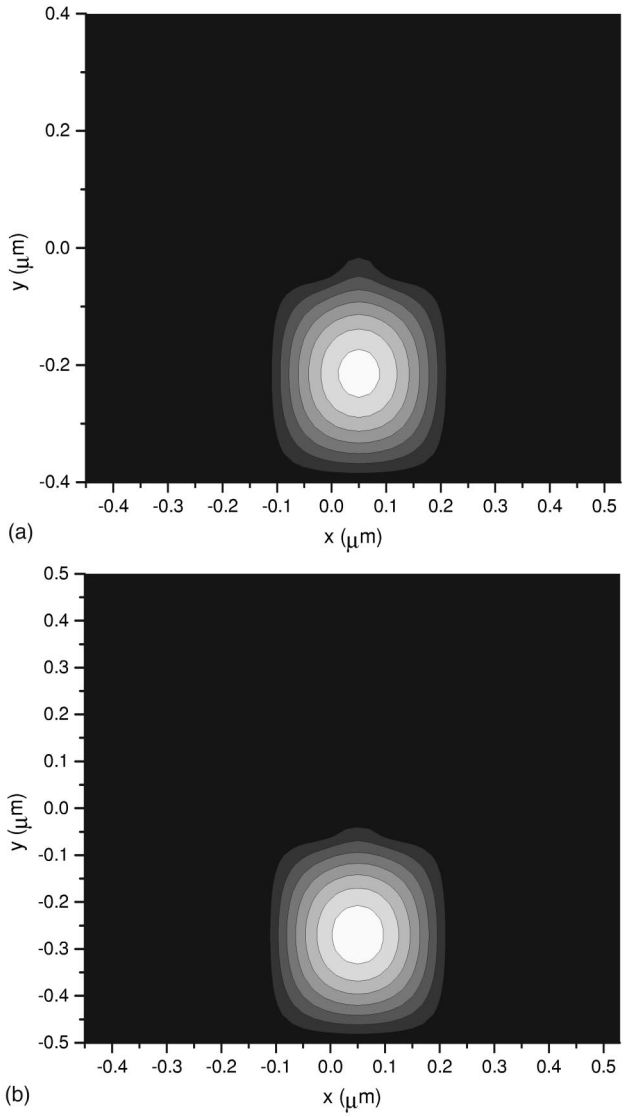

FIG. 5. Near electric field for the same grating of Fig. 4 and *s* polarization: (a) $h=0.4$ μm and $\lambda=0.509\,33$ μm, (b) $h=0.5$ μm and $\lambda=0.557\,33$ μm.

TABLE II. Resonant wavelengths λ (μm) for a gold grating of period $d=1$ μm, corresponding to SPP excitations.

n	$\theta_0=10°$	$\theta_0=20°$	$\theta_0=40°$
1	0.847	0.695	0.501
2	0.492	0.209	0.190
−1	1.182	1.349	1.647
−2	0.616	0.690	0.832
−3	0.463	0.497	0.573

peaks in a plot of $|\det[M]|^{-2}$ versus wavelength provide us with a good estimate of the resonant wavelengths of the cavity [19,20,11,6].

IV. RESULTS AND DISCUSSION

The examples below show the influence of the different types of resonances—SPP and SSR—in the power reflected from an infinite grating. The particular characteristics of the near field at resonant wavelengths and the influence of the finite conductivity of the gratings are also studied.

In Fig. 2 we plot the specular efficiency from an infinite perfectly conducting grating of period $d=1$ μm with bottle-shaped grooves of widths $c_1=0.35$ μm and $c_2=0.1$ μm. The grating is illuminated by a *p*-polarized plane wave impinging with an angle $\theta_0=10°$. The three curves correspond to different depths of the cavities, but in all cases the ratio, $h_1/h=0.9$, is maintained. For $\lambda \geqslant 1.174$, the only propagating order is the specular order and therefore, the total reflected power goes in that direction and all fluctuations are forbidden. Thus, we analyze the response of the grating for smaller wavelengths. In the range of λ considered in Fig. 2, the number of propagating orders goes from one to five. Let us note that more diffracted orders contribute to the total reflected power for small values of the wavelength than for higher values. The first significant feature to notice in Fig. 2 is that each curve has several minima. Some of these dips appear almost at the same positions for the different depths considered, but some of them are shifted. It could be expected that the anomalies related to the appearance/disappearance of a propagating order (SPP) do not depend on the depth of the cavities but only on the period of the grating and the incidence angle. On the other hand, the minima associated with the particular shape of the cavities (SSR) depend on their geometrical parameters, particularly the depth, so the positions of these dips are expected to vary from one curve to the other. Consequently, we can identify two different kinds of resonances: SPP and SSR. Since the neck of the cavities is narrow, we can compare the resonant wavelengths of the cavity with those calculated analytically for a perfectly conducting rectangular waveguide. In this case, the resonant wavelengths satisfy the condition $kh_1=n\pi$, where n is an integer. These values are listed in Table I for the depths h considered in Fig. 2. Comparing these values with the positions of the dips in Fig. 2, and taking into account that these wavelengths depend on the depth of the cavity, we can easily identify which of the resonant wavelengths correspond to SSR. The wavelengths listed in Table I for the rectangular waveguide are slightly greater than those of Fig. 2, and this is in agreement with the results obtained in [4] for a bivalued perfectly conducting cavity with circular cross section.

To confirm the nature of the different dips in Fig. 2, we have calculated the near field in a single period of the grating for the corresponding wavelengths, and this is shown as contour plots in Fig. 3. The black respresents the minimum intensity and the white represents the maximum intensity. For $h=1$ μm, we plot the near electric field for $\lambda=0.885\,67$ μm [Fig. 3(a)], and for $\lambda=0.586\,67$ μm [Fig. 3(b)]. We observe that in Fig. 3(a) the electric field has penetrated in the cavity, whereas in Fig. 3(b) the field is intensified on the surface. The field distribution in both cases suggests that the first case corresponds to a SSR and the second corresponds to a SPP excitation. A similar result was obtained by López-Rios *et al.* in [10] for a rectangular grating. Comparing Figs. 3(c) and 3(d), which correspond to $h=0.8$ μm, the same analysis can be made. In this case it is also clear that the dip at λ

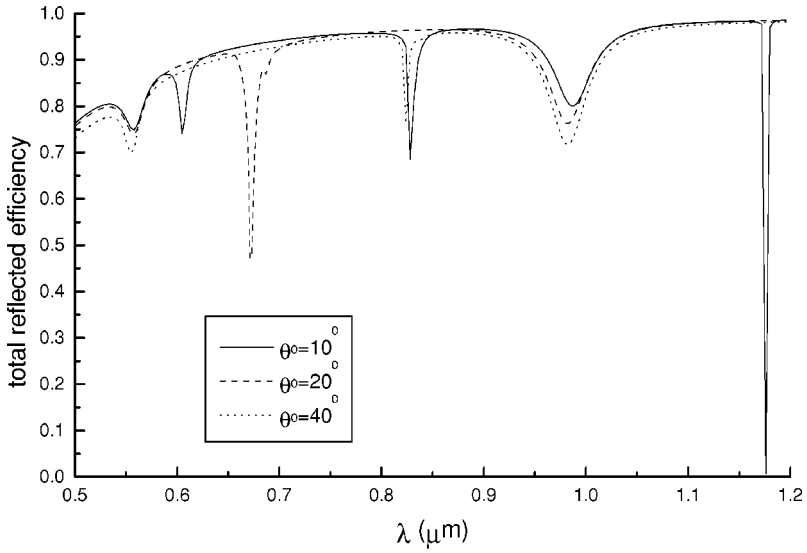

FIG. 6. Total reflected efficiency versus wavelength for a gold grating of period $d=1$ μm, with grooves of width $c_1=0.35$ μm, $c_2=0.1$ μm, $h=0.5$ μm, $h_1=0.9h$ and p polarization, for three different incidence angles: $\theta_0=10°$, 20°, and 40°.

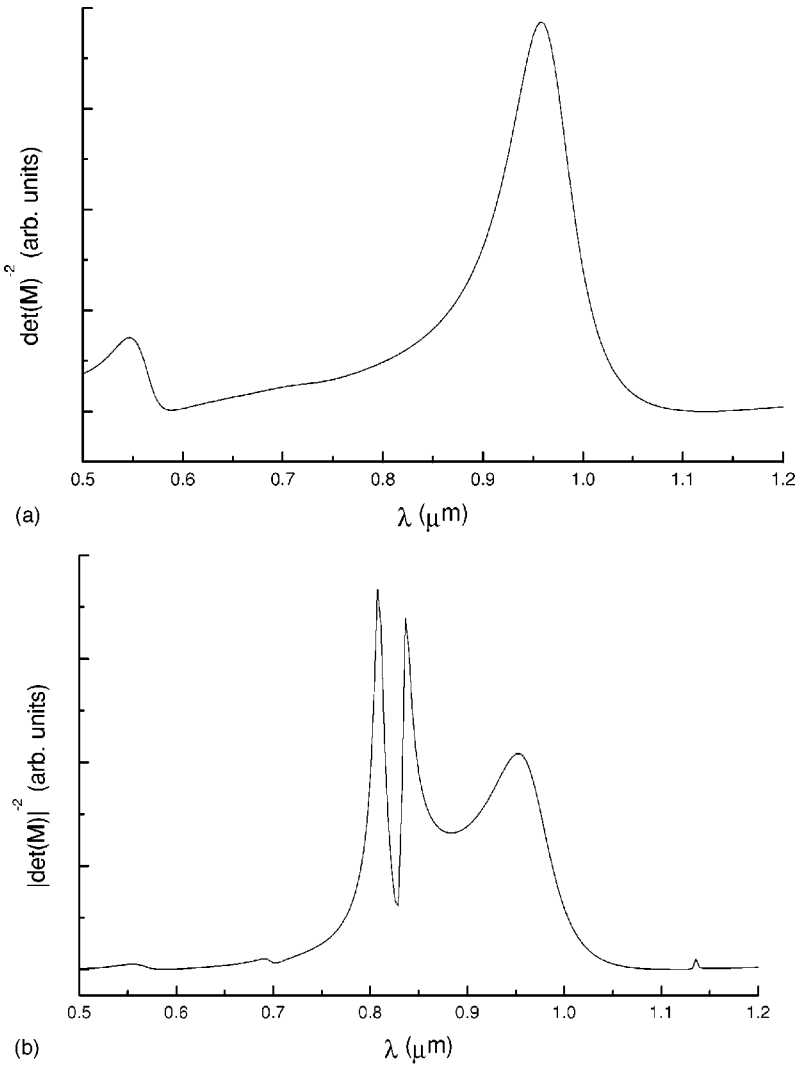

FIG. 7. $|\det(M)|^{-2}$ versus wavelength for a single bottle-shaped groove with parameters $c_1 = 0.35$ μm and $c_2 = 0.1$ μm, $h = 0.5$ μm, $h_1 = 0.9h$, on a gold surface. The incident light is p polarized.

$=0.7055$ μm [Fig. 3(c)] corresponds to a SSR and the dip at $\lambda = 0.586\,67$ μm [Fig. 3(d)] corresponds to a SPP.

In Fig. 4 we plot the specular efficiency versus the incident wavelength for the same grating considered in Fig. 2, but now illuminated by an s-polarized incident wave. The different curves correspond to different values of the depth: $h = 0.4$ μm and 0.5 μm. In the range of λ considered, only one dip for each h is observed. Since the position of the dip depends on the depth of the cavity, we associate this effect with a surface shape resonance. The reasons that account for the presence of a single dip in each curve are the following. On the one hand, there is no possibility of exciting a surface plasmon along the surface under s-polarized illumination, and therefore all the anomalies related to SPPs are not present in this case. On the other hand, the wavelengths associated with surface shape resonances are now different from those corresponding to p polarization. In the limiting case of a rectangular waveguide, the resonant wavelengths for the first modes are found by imposing the condition $v_{11}h_1 = n\pi$, instead of that used for the p case (see the Appendix for the definition of v_{11}). For the range of λ under consideration, the only resonant values resulting from the waveguide condition are $\lambda = 0.5$ μm (for $h = 0.4$) and $\lambda = 0.552$ μm (for $h = 0.5$), and it can be observed that these values coincide almost exactly with the positions of the dips in Fig. 4. These dips are more localized than those in Fig. 2 for p polarization, as it was already observed in [6].

To verify that the minima in Fig. 4 can be identified as SSR, we show in Fig. 5 contour plots of the near electric field for these cases. Fig. 5(a) corresponds to $h = 0.4$ μm and $\lambda = 0.509\,33$ μm, and Fig. 5(b) corresponds to $h = 0.5$ μm and $\lambda = 0.557\,33$ μm. In both cases the field is concentrated inside the cavity, with the highest intensity in its center. As it was shown in the previous example, this is a characteristic of SSR.

Having considered the ideal case of a perfectly conducting grating, we now study the more interesting and realistic case of lossy metals. The losses are included in the analysis applying the SIBC [17]. The refraction index ν at different wavelengths in the range under consideration was taken from Ref. [21], and then the curve $\nu(\lambda)$ was estimated by fitting these values with a second order polynomial. In the following figures, we consider a gold grating with bottle-shaped cavities. To find the wavelengths at which it is possible to excite a SPP for the grating studied, we solved the implicit equation

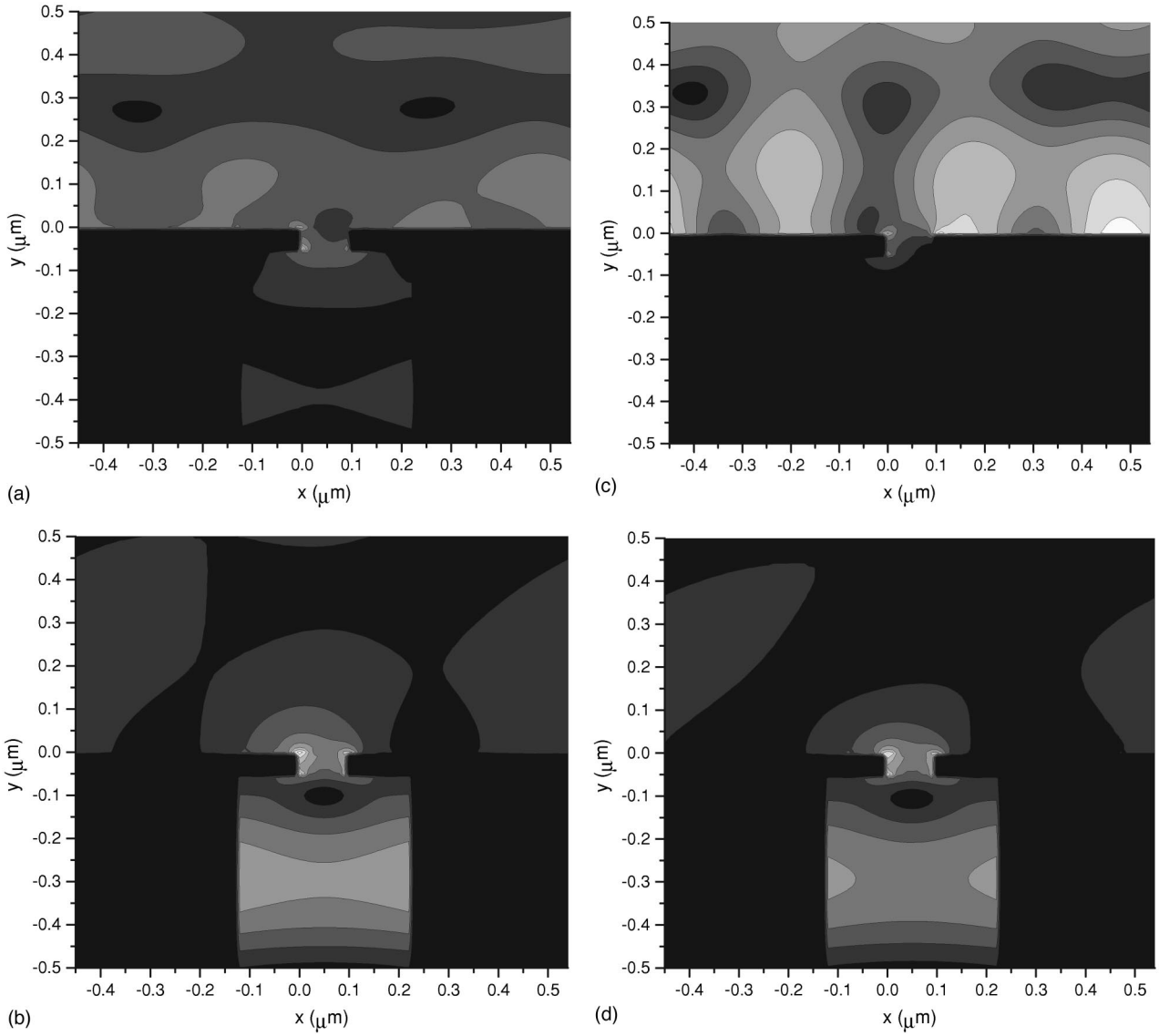

FIG. 8. Near electric field for the same grating of Fig. 6 and p polarization: (a) $\theta_0=10°$ and $\lambda=0.604$ μm, (b) $\theta_0=10°$ and $\lambda=0.988$ μm, (c) $\theta_0=20°$ and $\lambda=0.686$ μm, (d) $\theta_0=20°$ and $\lambda=0.98$ μm.

$$\left[\pm\sqrt{\frac{\nu(\lambda)^2}{1+\nu(\lambda)^2}}-\sin\theta_0\right]\frac{d}{n}-\lambda=0, \tag{11}$$

and some of the solutions of Eq. (11) are listed in Table II.

In Fig. 6 we plot the total reflected efficiency as a function of the incident wavelength, for a gold grating with cavities of $c_1=0.35$ μm, $c_2=0.1$ μm, $h=0.5$ μm, $h_1/h=0.9$, $d=1$ μm and incident p polarization, for three incidence angles: 10°, 20° and 40°. Notice that for a real metal, the minima represent power absorption, forbidden in the previous case of a perfect conductor. The dips in the solid line of Fig. 6 are moved with respect to those corresponding to the perfect conductor (dashed line in Fig. 2). As expected, the SPP excitations (see Table II) and the SSR now take place at different wavelengths. Comparing the three curves in Fig. 6, we can notice that some of the dips remain at almost the same positions, whereas some others move. Those minima that remain almost fixed when changing the angle of incidence are supposed to correspond to SSR since geometrical parameters are much more relevant for their excitation than incident conditions. However, a slight shift is also expected because at oblique incidence the projection of the wavelength in the (x,z) plane increases with the angle, and consequently the resonances occur for slightly smaller wavelengths. This behavior was already observed in [5]. On the other hand, the minima produced by a SPP excitation are expected to move with the angle of incidence, as is understood from Eq. (11).

To confirm that a certain dip corresponds to a SSR, it is important to solve the homogeneous problem. This calculation was done here for a bottle-shaped groove in a lossy metallic plane surface (see Sec. III). A similar problem was already solved for the perfect conductor case [6]. As explained in Sec. III, the last step of the solution process is to find the roots of the determinant of a complex matrix. Another possibility to identify the resonant wavelengths of the

cavity is to plot $|\det(M)|^{-2}$ versus wavelength, and the peaks in this curve represent resonant conditions of the structure [19,20,11,6]. The number of modal terms considered in the calculation is varied to identify each peak with a particular resonant mode. For instance, in Fig. 7(a) we consider only one modal term in the field expansions inside the cavity (gold surface with a groove of $c_1=0.35$ μm, $c_2=0.1$ μm, $h=0.5$ μm, $h_1=0.9h$, *p*-polarization case). This implies that the two peaks correspond to the lower symmetric modes of the groove. For Fig. 7(b) two modes had been included in the calculation, and it can be noted that in addition to the maxima observed in Fig. 7(a) there are new peaks that can be associated with higher order modes. Since the surface shape resonances do not depend on the incidence conditions, the peaks in Fig. 7 are associated with resonant wavelengths, for any angle of incidence. Particularly, if we compare this curve with Fig. 6, it can be noticed that two of the dips that do not move with the angle of incidence ($\lambda\approx0.55$ μm and $\lambda\approx0.98$ μm) appear at the wavelengths of the peaks in Fig. 7(a). There is another dip at $\lambda\approx0.83$ μm, which in principle can be associated with one of the peaks in Fig. 7(b). The near electric field for the case of Fig. 6 is shown in Fig. 8, for several wavelengths corresponding to minima in the reflected efficiency: $\theta_0=10°$ and $\lambda=0.604$ μm [Fig. 8(a)], $\theta_0=10°$ and $\lambda=0.988$ μm [Fig. 8(b)], $\theta_0=20°$ and $\lambda=0.686$ μm [Fig. 8(c)], and $\theta_0=20°$ and $\lambda=0.980$ μm [Fig. 8(d)]. As observed in Fig. 3 for the perfectly conducting surface, in the case of surface shape resonances [Figs. 8(b) and 8(d)], the field enters inside the cavity, where the maximum intensity is found. On the other hand, for the SPP excitations [Figs. 8(a) and 8(c)], the field is more intense on the surface, and slightly penetrates into the cavity. However, there are dips in Fig. 6 that can hardly be identified with one of the two types of resonances, as, for example, the dips at $\lambda\approx0.55$. Even though these dips seem to be associated with a SSR, the near field distribution suggests that this is a hybrid mode. In Fig. 9 we show the near field for the case in Fig. 6, for $\theta_0=10°$ and $\lambda=0.558$ μm [Fig. 9(a)] and for $\theta_0=40°$ and $\lambda=0.55$ μm [Fig. 9(b)]. In this type of resonance the near field exhibits a character intermediate between the typical behaviors corresponding to SPP and SSR, as shown in Fig. 8. These hybrid resonances had already been observed for lamellar gratings [10].

In the last example we consider the *s*-polarization mode. In Fig. 10(a) we plot the total reflected efficiency for a gold grating with cavities of widths $c_1=0.35$ μm, $c_2=0.1$ μm, $h=0.5$ μm, $h_1/h=0.9$, $d=1$ μm, and $\theta_0=10°$. Comparing this curve with that for the perfect conductor (Fig. 4), it can be noticed that the dip is now shifted and less localized. Both changes are associated with the finite conductivity of the metal: the SSR depends not only on the geometrical parameters but also on the material of the structure, as is confirmed in Fig. 10(b) where we plot $|\det(M)|^{-2}$ for a single cavity in the *s* mode. The location of the peak coincides with the position of the dip in Fig. 10(a). In Fig. 10(c), the SSR character of this resonance is confirmed, since for this wavelength $\lambda=0.6458$ μm, most of the intensity is concentrated inside the cavity.

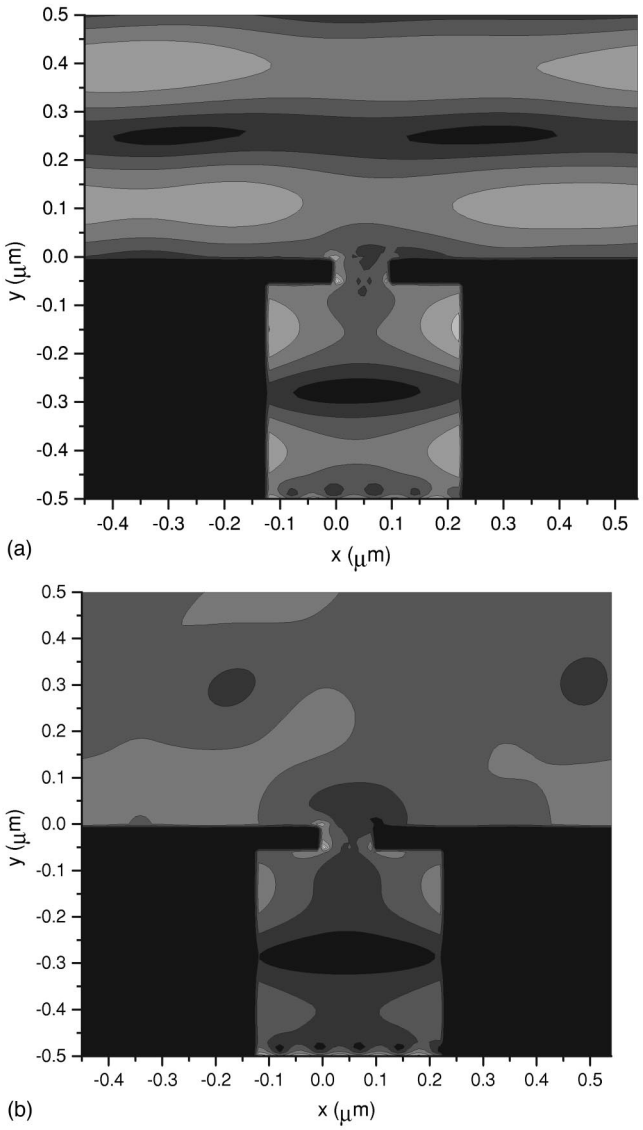

FIG. 9. Near electric field for the same grating of Fig. 6 and *p* polarization: (a) $\theta_0=10°$ and $\lambda=0.558$ μm, (b) $\theta_0=40°$ and $\lambda=0.55$ μm.

V. CONCLUSION

In this paper we have solved the diffraction problem from an infinite grating with bottle-shaped cavities on a metallic surface, for *s* and *p* polarizations. We believe that the most interesting contribution of this paper is the introduction of the lossy characterisitic of a real metal, and the effects that this property produces in the behavior of the electromagnetic field. We used the modal approach, which is particularly suitable for this geometry, and the surface impedance boundary condition to take into account the losses in the metal. We also solved the homogeneous problem of a single cavity in a plane metallic surface using the same technique. The results shown place particular emphasis on the excitation of surface plasmon polaritons and surface shape resonances in this type of bivalued structures. We verified the different nature of the

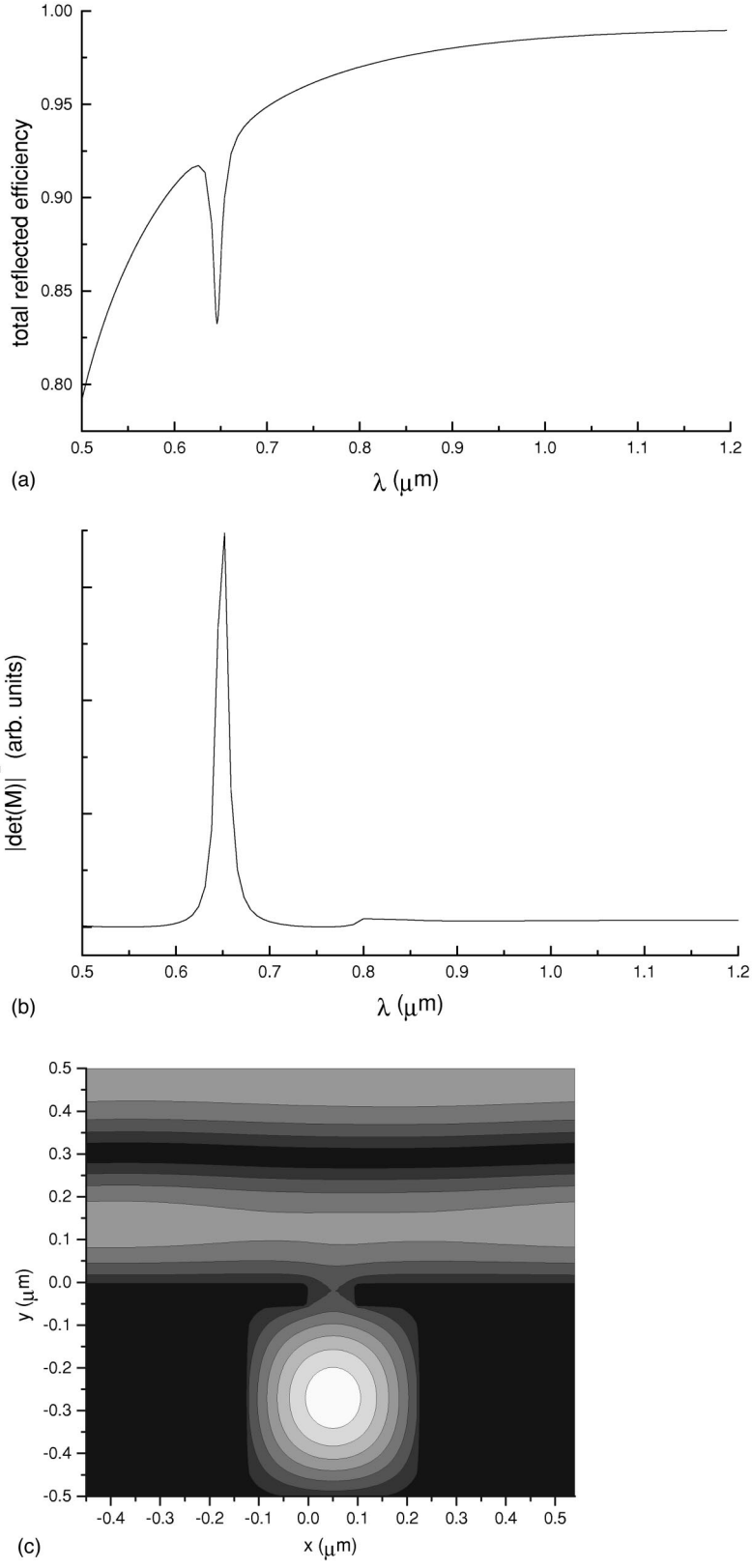

FIG. 10. (a) Total reflected efficiency versus wavelength for a gold grating of period $d=1$ μm with grooves of width $c_1=0.35$ μm, $c_2=0.1$ μm, $h=0.5$ μm, $h_1=0.9h$, $\theta_0=10°$, and s polarization, (b) $|\det(M)|^{-2}$ versus wavelength for a single groove with the same parameters of (a), and (c) near electric field for the same grating of (a) and for $\lambda=0.6458$ μm.

resonances that appear as dips in the reflected efficiency, by calculating the eigenmodes of a single cavity and also by analyzing the near field distribution. The existence of hybrid modes was also addressed for the gratings studied. The results suggest that the resonant wavelenghts and the proximity between them can be controlled by changing the angle of incidence and/or the depth of the cavities. A comparison between the results obtained for a perfectly conducting surface and for a lossy metal was also provided, and the differences between them were discussed.

ACKNOWLEDGMENTS

This work was supported by Agencia para la Promoción Científica y Tecnológica (APCYT) under Grant No. BID802/OC-AR-PICT03-04457 and by Universidad de Buenos Aires (UBA).

APPENDIX: EXPLICIT EXPRESSIONS OF THE MODAL FUNCTIONS

$$U^s_{m,j}(x)=\sin[u^s_{m,j}(x-x_j)]+\eta^s u^s_{m,j}\cos[u^s_{m,j}(x-x_j)],\quad j=1,2, \tag{A1}$$

$$U^p_{m,j}(x)=\frac{\eta^p}{u^p_{m,j}}\sin[u^p_{m,j}(x-x_j)]+\cos[u^p_{m,j}(x-x_j)],\quad j=1,2, \tag{A2}$$

$$w^q_{m,1}(y)=A^q[K^q_m\cos(v^q_{m,1}y)+\sin(v^q_{m,1}y)],\quad q=s,p, \tag{A3}$$

$$w^q_{m,2}(y)=a^q_m\cos(v^q_{m,2}y)+b^q_m\sin(v^q_{m,2}y),\quad q=s,p, \tag{A4}$$

where $x_1=-(c_1-c_2)/2$, $x_2=0$, $(v^q_{m,j})^2=k^2-(u^q_{m,j})^2$,

$$\eta^q=\begin{cases} i\mathcal{Z}/k=i/\nu k & \text{if } q=s \\ \mathcal{Z}k/i=k/\nu i & \text{if } q=p, \end{cases} \tag{A5}$$

$$K^s_m=\frac{\eta^s v^s_{m,1}\cos(v^s_{m,1}h)+\sin(v^s_{m,1}h)}{\cos(v^s_{m,1}h)-\eta^s v^s_{m,1}\sin(v^s_{m,1}h)}, \tag{A6}$$

$$K^p_m=\frac{\eta^p\sin(v^p_{m,1}h)+v^p_{m,1}\cos(v^p_{m,1}h)}{\eta^p\cos(v^p_{m,1}h)-v^p_{m,1}\sin(v^p_{m,1}h)}, \tag{A7}$$

and $u^q_{m,j}$ are determined by an eigenvalues equation for each polarization:

$$\tan(u^s_{m,j}c_j)=\frac{2\eta^s u^s_{m,j}}{(\eta^s u^s_{m,j})^2-1},\qquad \tan(u^p_{m,j}c_j)=\frac{2\eta^p u^p_{m,j}}{(u^p_{m,j})^2-(\eta^p)^2}. \tag{A8}$$

[1] V.M. Agranovich and D.L. Mills, *Surface Polaritons* (North-Holland, Amsterdam, 1982).
[2] A. Hessel and A.A. Oliner, Appl. Opt. **4**, 1275 (1965).
[3] M.C. Hutley, *Diffraction Gratings* (Academic Press, London, 1982), Chap. 6.
[4] C.I. Valencia and R.A. Depine, Opt. Commun. **159**, 254 (1999).
[5] D.C. Skigin and R.A. Depine, Phys. Rev. E **59**, 3661 (1999).
[6] R.A. Depine and D.C. Skigin, Phys. Rev. E **61**, 4479 (2000).
[7] J.R. Andrewartha, J.R. Fox, and I.J. Wilson, Opt. Acta **26**, 69 (1979).
[8] J.R. Andrewartha, J.R. Fox, and I.J. Wilson, Opt. Acta **26**, 197 (1979).
[9] A. Wirgin and A.A. Maradudin, Phys. Rev. B **31**, 5573 (1985).
[10] T. López-Rios, D. Mendoza, F.J. García-Vidal, J. Sánchez-Dehesa, and B. Pannetier, Phys. Rev. Lett. **81**, 665 (1998).
[11] A.A. Maradudin, A.V. Shchegrov, and T.A. Leskova, Opt. Commun. **135**, 352 (1997).
[12] R.W. Ziolkowski and J.B. Grant, IEEE Trans. Antennas Propag. **35**, 504 (1987).
[13] D. Colak, I. Nosich, and A. Altintas, IEEE Trans. Antennas Propag. **41**, 1551 (1993).
[14] D. Colak, I. Nosich, and A. Altintas, IEEE Trans. Antennas Propag. **43**, 440 (1995).
[15] V.V. Veremey and V.P. Shestopalov, Radio Sci. **26**, 631 (1991).
[16] V.V. Veremey and R. Mittra, IEEE Trans. Antennas Propag. **46,4**, 494 (1998).
[17] R.A. Depine, in *Scattering in Volumes and Surfaces*, edited by M. Nieto-Vesperinas and J.C. Dainty (North-Holland, Amsterdam, 1990), pp. 239–253.
[18] R.A. Depine and D.C. Skigin, J. Opt. Soc. Am. A **11**, 2844 (1994).
[19] A.A. Maradudin, P. Ryan, and A.R. McGurn, Phys. Rev. B **38**, 3068 (1988).
[20] A.V. Shchegrov and A.A. Maradudin, Appl. Phys. Lett. **67**, 3090 (1995).
[21] G. Hass, in *Mirror Coatings*, Applied Optics and Optical Engineering, edited by R. Kingslake (Academic Press, New York, 1996), Vol. 3, p. 316.